Kovove Mater. 49 2011 253–264
DOI: 10.4149/km_2011_4_253

Solidification of A356 Al alloy: Experimental study and modeling

M. O. Shabani[1]*, A. Mazahery[2], A. Bahmani[3], P. Davami[3], N. Varahram[3]

[1] *Materials and Energy Research Center (MERC), Tehran, Iran*
[2] *School of Metallurgy and Materials Engineering, University of Tehran, Tehran, Iran*
[3] *Department of Materials Engineering, Sharif University of Technology, Tehran, Iran*

Received 1 June 2010, received in revised form 26 October 2010, accepted 27 October 2010

Abstract

While it is well recognized that microstructure controls the physical and mechanical properties of a material, the complexity of the microstructure often makes it difficult to be simulated by analytical or numerical techniques. In this paper we present a suitable approach to compute microstructures within a casting using the finite element technique. This technique allows implementing microstructure data from experiments and equations that describe microstructure as function of local solidification parameters. The comparison of this model's predictions with the ones in the literature and also experimental measurements of secondary dendrite arm spacing, average length and diameter of silicon rods for A356 alloy are presented in this work. It is revealed that predictions of this study are consistent with the other models and experimental measurements for A356 alloy. The results of this research were also used in order to form analytical equations followed with solidification codes for SUT (Sharif University Technology) software.

K e y w o r d s: A356, microstructure, modeling

1. Introduction

Cast aluminum-silicon alloys have widespread applications, especially in the aerospace and automotive industries. These foundry alloys have an excellent combination of castability and mechanical properties, as well as good corrosion resistance and weldability [1–3]. Successful development of application of aluminum casting parts needs high strength and elongation. Grain size and its morphology, dendrite arm spacing (DAS), size and distribution of secondary phases are effective parameters, which control mechanical properties of casting parts [4, 5]. The quality of the microstructure of aluminum parts depends on chemical composition, melting process, casting process and solidification rate [6–8]. Solidification begins with the development of primary aluminum dendrite network in majority of aluminum casting alloys. The secondary dendrite arm spacing (SDAS) depends on chemical composition of the alloy, cooling rate, local solidification time and temperature gradient [1, 9]. The SDAS controls the size and the distribution of porosity and intermetallic particles in the casting. As SDAS becomes smaller, porosity and second phase constituents are dispersed more finely and evenly. This refinement of the microstructure leads to substantial improvement in mechanical properties [1, 10, 11].

In 1966, Oldfield proposed that the heat source term in the heat transfer equation could be represented by the function of nucleation rate and growth velocity of crystal grains, and attempted to simulate the solidification microstructure of gray cast iron. Yet the micro simulation developed slowly, confined by the corresponding macro simulation during following decades [12].

It is well established that under most conditions of solidification, the dendritic morphology is the dominant characteristic of the microstructure of off-eutectic alloys. Fine dendritic microstructures in castings, characterized by the dendrite arm spacing, are recognized to have superior mechanical properties than coarser ones, particularly when considering the tensile strength and ductility. Much research has been devoted to the definition of the factors affecting the fine-

*Corresponding author: tel.: +98 912 563 6709; fax: +98 261 6201888; e-mail address: vahid_ostadshabany@yahoo.com

ness of the dendritic structure. Numerous solidification studies have been reported with regard to characterizing primary and secondary dendrite arm spacing as function of alloy solute concentration, tip growth rate and temperature gradient ahead of the macroscopic solidification front [13]. An eutectic constituent, consisting of aluminum solid solution and silicon, then grows between the primary dendritic networks. The morphology of the silicon phase is either rod-like or plate-like depending on whether the melt has been treated with modifiers such as sodium or strontium. In a two dimensional metallographic section, the silicon rods look like particles and the silicon plates look like rods. The morphology of the primary aluminum solid solution is described by the primary and secondary dendrite arm spacing, DAS and SDAS, respectively. The morphology of the silicon phase is described by the silicon rod particle diameter, silicon spacing and silicon rod length. In this paper, each of these length scales is discussed in detail. Analytical equations are generated for these length scales and incorporated in commercial software for the prediction of microstructure in shape castings [14].

2. Experimental procedure

Approximately 4.5 kg of A356 was charged into the crucible made from cast iron and heated up to above 720 ℃ and then poured into a sand mould representing a step casting. For modification purposes, strontium (100 ppm) was added between 680–700 ℃ in the form of Al10%Sr master alloy. The chemical analysis of the ingot used to make the step castings is presented in Table 1. Fifteen thermocouples were implemented to experimentally measure local cooling rates. The cooling rate and temperature gradient obtained from simulation are validated by experimental cooling curve. Figure 1 shows the scale drawing for the step casting and indicates the position of each thermocouple being inserted to a depth of 20 mm. The casting was gated from the side of the riser. The casting was then sectioned and samples were extracted from steps 1 through 5.

For microstructure analysis the samples were prepared by grinding through 80, 120, 200, 400, 800, 1000 and 2000 grit papers followed by polishing and etched with HF %4. Micrographs of each sample were taken by optical microscopy. The A356 alloy is a hypo-eutectic alloy consisting of primary α-Al dendrite and eutectic Si particles. The images were then analyzed using a commercial image-analysis software package. Quantitative metallography was conducted by a Clemex Image Analysis system (Clemex CIR^{TM} 3.5). The DAS and SDAS were obtained by a linear intercept method where the line is chosen to intersect a series of well-defined dendrite arms. Most of the images were taken at a magnification of 50×, 100× and 200×.

T a b l e 1. Chemical analysis of the ingot used for the step castings (wt.%)

Si	Fe	Cu	Mn	Mg	Zn	Ti	Cr	Ni	Pb	Sn
6.91	0.4	0.25	0.2	0.33	0.31	0.02	0.01	0.05	0.1	<0.01

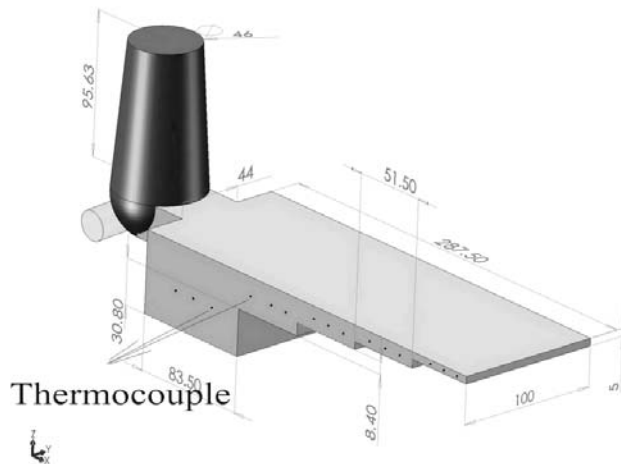

Fig. 1. Scale drawing of the step casting.

The DAS, SDAS, length and diameter of silicon particles were measured and analyzed as function of the cooling rate. The experimental results were compared to simulation results.

3. Prediction of microstructure

3.1. Primary and secondary dendrite arm spacing

Among the theoretical models existing in the literature only those proposed by Hunt and Lu [15] for primary spacing and Bouchard and Kirkaldy [16] for primary and secondary spacing assume solidification in unsteady-state heat flow conditions. Hunt, Kurz and Trivedi have derived primary spacing formulas, which are applied for steady-state conditions [17, 18]. The theoretical models for determination of dendrite spacing proposed by these authors are shown in Equations:

$$d_1 = 4.3 \left(\frac{\Gamma \Delta T D}{G^2 V k_0} \right)^{0.25} \tag{1}$$

and for A356 alloy:

$$d_1 = 70.33 G^{-0.35} V^{0.42} \text{ for } V(G/10000)^{-0.67} < 10^{-3},$$

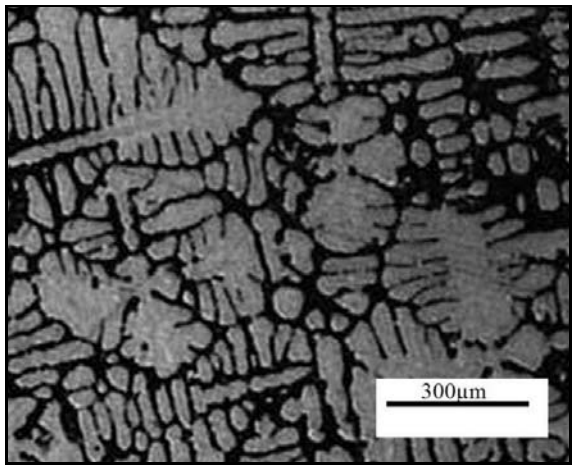

Fig. 2. Optical micrograph of a sample for the cooling rate of 0.1 (°C s^{-1}).

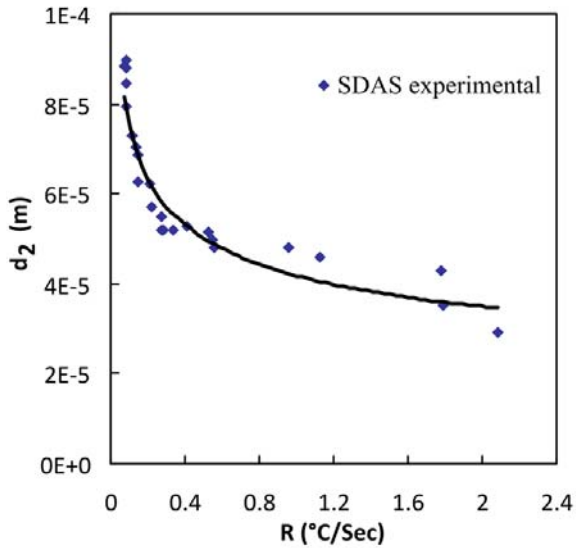

Fig. 3. Secondary dendrite arm spacing as a function of cooling rate for A356 alloy.

$$d_1 = 0.0576V^{0.94} \qquad \text{for } V(G/10000)^{-0.67} > 10^{-3}, \tag{2}$$

where d_1 is the primary dendrite arm spacing, Γ is the Gibbs-Thomson coefficient, k_0 is the solute partition coefficient, D is the liquid solute diffusivity, ΔT is the difference between the liquidus and solidus equilibrium temperature, V is the dendrite tip growth rate, G is the temperature gradient in front of the liquidus isotherm [14–18].

Figure 2 shows an optical micrograph for a cooling rate of 0.1 (°C s^{-1}). As can be seen, this picture exhibited an ordinary dendrite structure consisting of primary α-Al dendrites and eutectic. Numerous solidification studies have been developed aiming to characterize the dendrite arm spacing under experimental conditions involving solidification in steady-state heat flow and those in the unsteady-state regime. The latter case is of prime importance, since it is relevant for the majority of industrial solidification processes. In this case, which is the focus of this article, the secondary dendrite arm spacing (d_2) is usually expressed as a function of local solidification time (t_f), where M and K are constants [19]:

$$d_2 = K(Mt_f)^{1/3}. \tag{3}$$

The SDAS (d_2) was measured and analyzed as the function of the cooling rate using image analysis. The variation of d_2 with cooling rate (R) is presented in Fig. 3.

For A356 alloy, if we consider temperature differ-

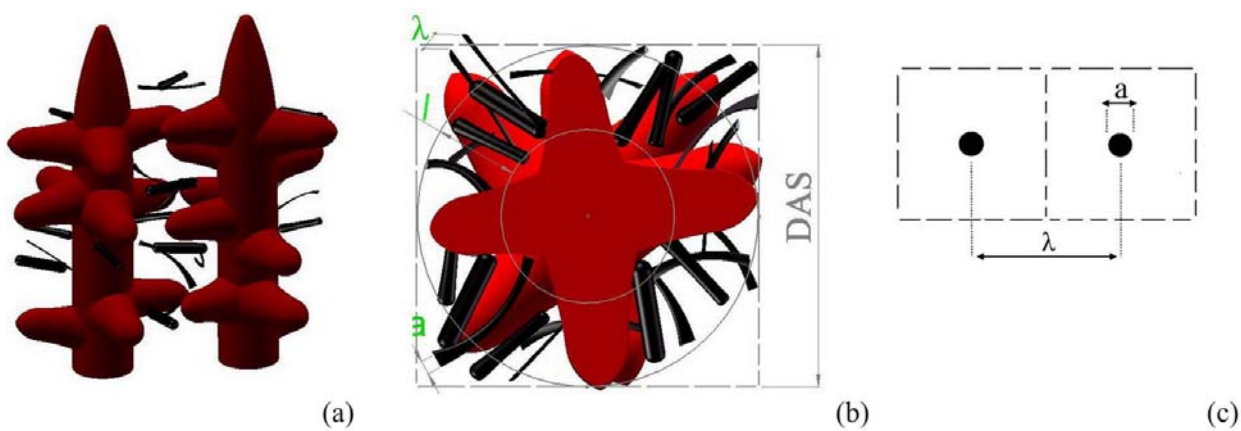

Fig. 4. Schematic diagram showing the length scales that characterize the morphology of primary dendrites (a), the relationship between the primary dendrite size and the average length of the silicon phase (b), and the relationship between spacing and diameter of silicon (c).

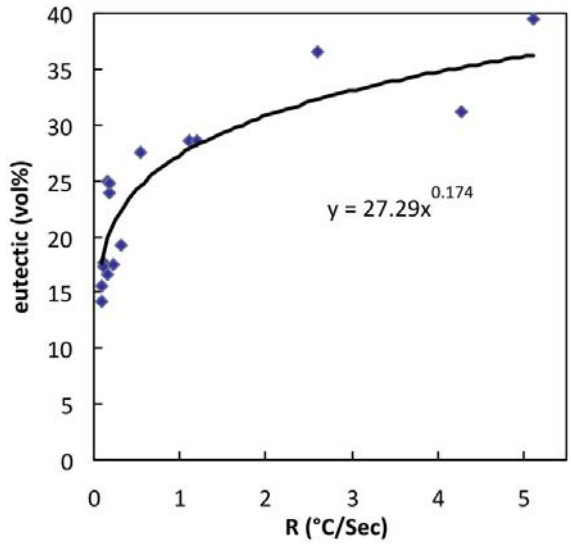

Fig. 5. Eutectic volume percentage as a function of cooling rate for A356 alloy.

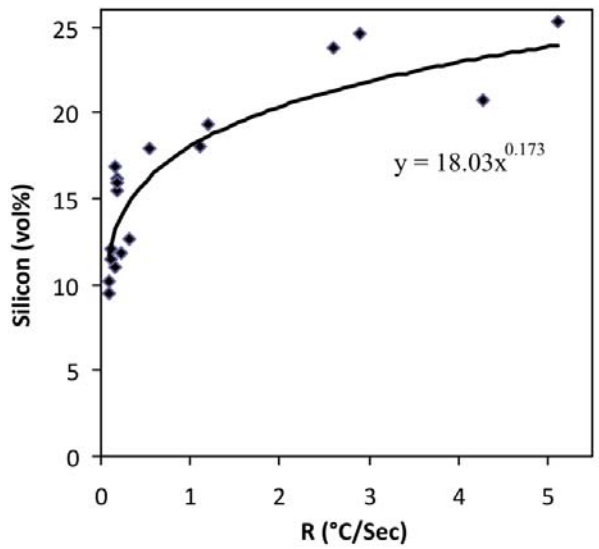

Fig. 6. Silicon volume percentage as a function of cooling rate for A356 alloy.

ence between liquidus and solidus 60, then:

$$t_{\mathrm{f}} = \frac{60}{R}, \tag{4}$$

$$d_2 = 10.4(t_{\mathrm{f}})^{1/3}. \tag{5}$$

3.2. Eutectic

Length scales that characterize the morphology of aluminum-rich dendrites are presented in Fig. 4, where the black phase is the silicon phase that branches by a twinning mechanism. The average length and diameter of silicon rods are defined by l and a, respectively. Knowing the volume fractions of the primary dendrite phase, silicon and eutectic, the average length of the silicon rods can be related to the primary dendrite size based on simple geometric considerations. The variations of the eutectic volume percentage and silicon volume percentage with cooling rate are shown in Figs. 5 and 6. Fitting these experimental data leads to Eqs. (6) and (7) and finally to geometrically consistent equations for the length and diameter of silicon rods (8) to (11).

$$V_{\mathrm{eutectic}} = 27.29R^{0.174}, \tag{6}$$

$$V_{\mathrm{silicon}} = 18.03R^{0.173}, \tag{7}$$

$$V_{\mathrm{eutectic}} = 1 - \frac{\pi(d_1/2 - l)^2}{d_1^2}, \tag{8}$$

$$l = d_1\left(\frac{1}{2} - \left(\frac{1 - V_{\mathrm{eutectic}}}{\pi}\right)^{0.5}\right), \tag{9}$$

$$V_{\mathrm{silicon}} = \frac{\pi a^2/4}{\lambda_{\mathrm{Si}}^2}, \tag{10}$$

$$a = 2\lambda_{\mathrm{Si}}\left(\frac{V_{\mathrm{silicon}}}{\pi}\right)^{0.5}, \tag{11}$$

where λ_{Si} is silicon rod spacing and can be obtained from the following form of growth law [14]:

$$\lambda_{\mathrm{Si}} = 0.16V^{-0.446}. \tag{12}$$

Equations (2), (5), (6), (7), (9), (11) and (12) are incorporated into the solidification software code for computation of microstructure features.

4. Validation of the model

Figure 7 shows the variation of the primary DAS with cooling rate for two different values of the temperature gradient, e.g. $G = 50$ and $G = 200\,^{\circ}\mathrm{C\,m^{-1}}$. The simulated results based on Kurz-Fisher's model [18] are consistent with experimental measurements of DAS in the step casting, suggesting that columnar dendritic growth occurred. For $G = 200\,^{\circ}\mathrm{C\,m^{-1}}$ the Peres model [13] agrees well to both simulated and experimental results, while for $G = 50\,^{\circ}\mathrm{C\,s^{-1}}$ and cooling rates $R < 0.5\,^{\circ}\mathrm{C\,s^{-1}}$ this was not the case. It seems that Kurz-Fisher's model is better suited to describe

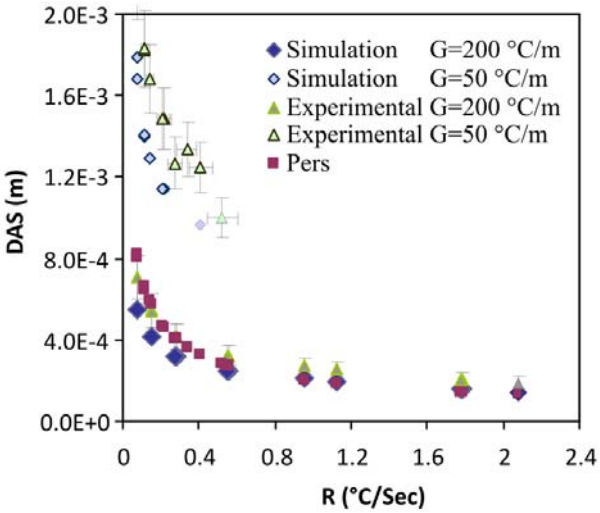

Fig. 7. Comparison of the model's predictions with experimental measurements of primary dendrite arm spacing for A356 alloy.

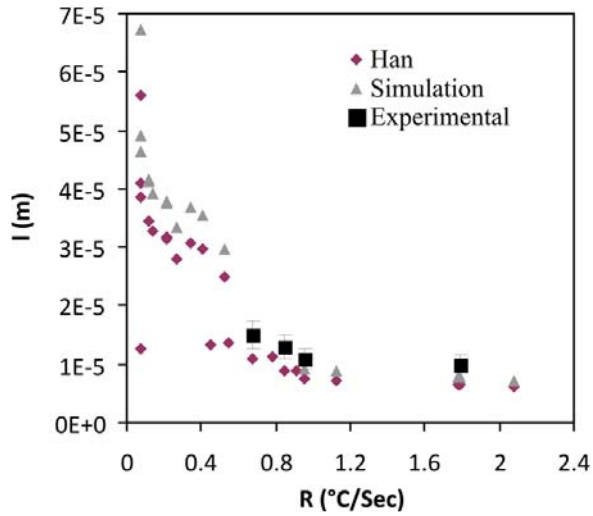

Fig. 9. Comparison of the model's predictions with experimental measurements of average length of silicon rods for A356 alloy.

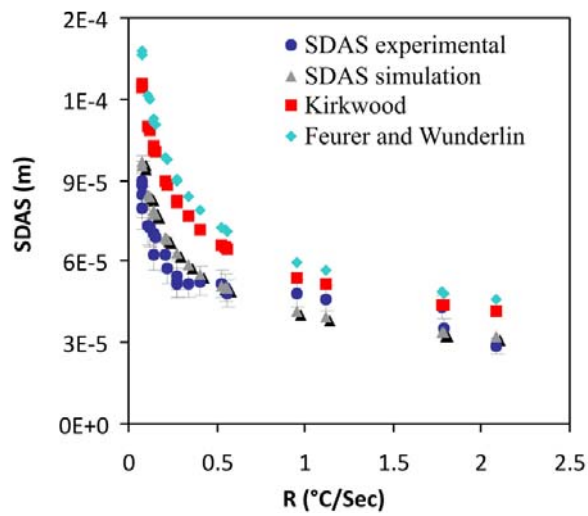

Fig. 8. Comparison of the model's predictions with experimental measurements of secondary dendrite arm spacing for A356 alloy.

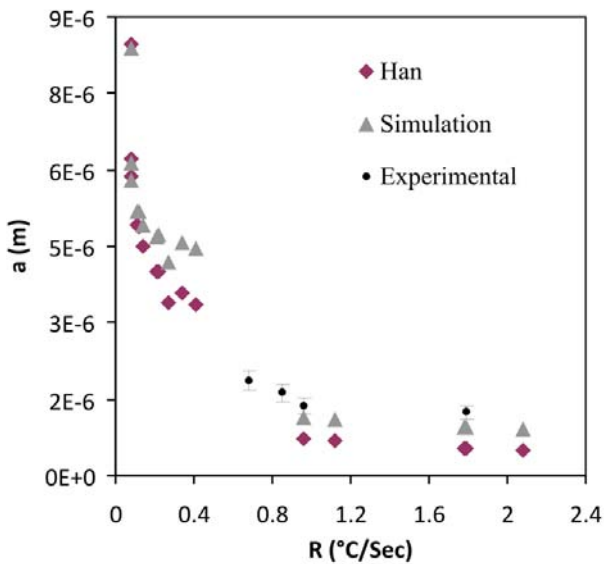

Fig. 10. Comparison of the model's predictions with experimental measurements of silicon rod diameter for A356 alloy.

the dependence of the primary dendrite arm spacing on both, cooling rate and temperature gradient.

Comparison of the model's predictions with experimental measurements of secondary dendrite arm spacing for A356 alloy is displayed in Fig. 8. The simulated results based on Pedro's model [17] are consistent with experimental measurements of DAS in the step casting. The models proposed by Kirkwood [20] and Feurer and Wunderlin [13] give slightly higher values.

Comparison of the model's predictions with experimental measurements of the average length of silicon rods for A356 alloy is shown in Fig. 9. The agreement is fairly good. The results from Han's model are also given. Han's assumption that the volume fraction of the eutectic is independent on the cooling rate leads to slightly lower values of the average length of silicon rods. Figure 10 shows the comparison of the model's predictions with experimental measurements of the silicon rod diameter for A356 alloy, along with calculations using Han's model. The volume fraction of the silicon phase depends on the cooling rate in this model, while it is constant in Han's model. As above, a better agreement with experimental results is achieved when the volume fraction of the silicon phase is a func-

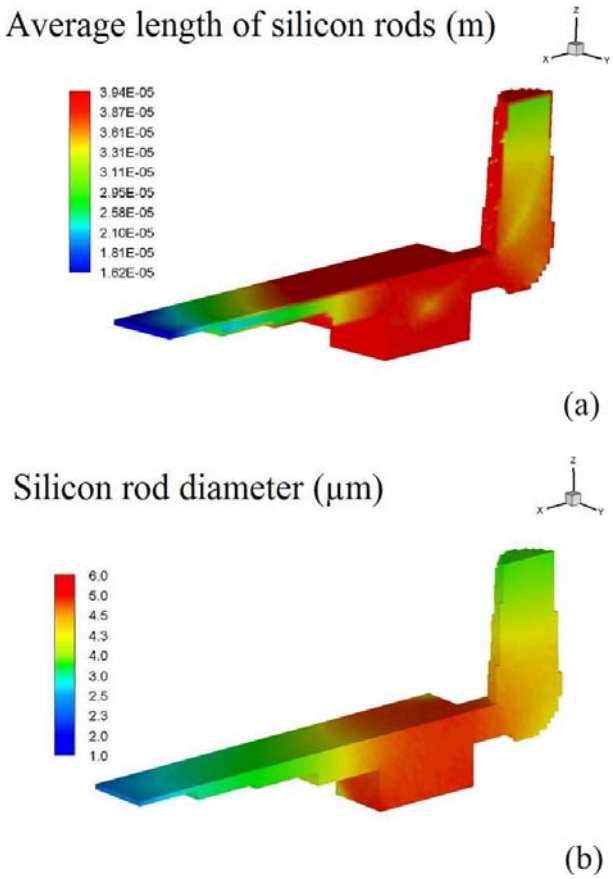

Fig. 11. Modeled distribution of the average length of silicon rods (a) and the silicon rod diameter (b) inside the step casting.

tion of the cooling rate. Finally, Fig. 11 resumes the simulation results for the step casting from alloy A356, showing the distribution of the average length of silicon rods and the silicon rod diameter inside the entire casting.

5. Conclusions

1. Microstructure modeling of solidification in A356 alloy was developed for the prediction of the primary dendrite spacing, secondary dendrite spacing and silicon rod length, diameter and spacing as function of local solidification conditions.

2. Microstructure modeling was performed by incorporating adequate analytical equations into the post processing module of commercial solidification software.

3. The model was used to compute the primary and secondary dendrite arm spacing of aluminum solid solution as well as the morphology of the eutectic Si phase within a step casting.

4. The model results were compared to experimental measurements and showed satisfactory agreement. The modeling approach is convenient for determining the micro structural length scales in A356 aluminum alloy casting that are needed for mechanical property and component life prediction models.

References

[1] CROSELEY, P. E.—MONDOLFO, L. F.: AFS Trans., *74*, 1966, p. 53.
[2] KORI, S. A.—MURTY, B. S.—CHAKRABORTY, M.: Mater. Sci. Eng. A., *283*, 2000, p. 94. doi:10.1016/S0921-5093(99)00794-7
[3] HEUSLER, L.—SCHNEIDER, W.—LIGHT, J.: Met., *2*, 2002, p. 17.
[4] GOKHALE, A. M.—PATEL, G. R.: Mater. Sci. Eng. A., *392*, 2005, p. 184. doi:10.1016/j.msea.2004.09.051
[5] JIAN, X.—XU, H.—MEEK, T. T.—HAN, Q.: Mater. Lett., *59*, 2005, p. 190. doi:10.1016/j.matlet.2004.09.027
[6] GANDIN, CH. A.: Iron Inst. Steel Jpn., *40*, 2000, p. 971.
[7] SHABESTARI, S. G.—MOEMENI, H.: Mater. Proc. Technol., *153*, 2004, p. 193. doi:10.1016/j.jmatprotec.2004.04.302
[8] KASHYAP, K. T.—MURALI, S.—MURTHY, K. S. S.: Mater. Sci. Technol., *9*, 1993, p. 189.
[9] VELDMAN, N. L. M.—DAHLE, A. K.—STJOHN, D. H.—ARNBERG, L.: Metall. Mater. Trans., *32A*, 2001, p. 147. doi:10.1007/s11661-001-0110-1
[10] GOWRI, S.—SAMUEL, F. H.: Metall. Mater. Trans. A, *25A*, 1994, p. 437. doi:10.1007/BF02647989
[11] WANG, Q. G.—DAVIDSON, C. J.: J. Mater. Sci., *36*, 2001, p. 739. doi:10.1023/A:1004801327556
[12] ZHAO, Y.—HOU, H.: Institute of Physics Publishing, Conference Series, *29*, 2006, p. 219.
[13] PERES, M. D.—SIQUEIRA, C. A.—GARCIA, A.: J. Alloy Comp., *381*, 2004, p. 168. doi:10.1016/j.jallcom.2004.03.107
[14] HAN, Q.—VISWANATHAN, S.: Light Metals 2000. Ed.: Peterson, R. D. Warrendale, PA, The Minerals, Metals & Materials Society 2000, p. 609.
[15] HUNT, J. D.—LU, S. Z.: Metall. Mater. Trans. A, *27*, 1996, p. 611. doi:10.1007/BF02648950
[16] BOUCHARD, D.—KIRKALDY, J. S.: Metall. Mater. Trans. B, *28*, 1997, p. 651. doi:10.1007/s11663-997-0039-x
[17] KURZ, W.—FISHER, J. D.: Acta Metall., *29*, 1981, p. 11. doi:10.1016/0001-6160(81)90082-1
[18] KURZ, W.—FISHER, J. D.: Fundamentals of Solidification. Uetikon Zürich, Trans. Tech. Publications Ltd. 1992.
[19] PEDRO, R. G.—JOSÉ, E.—SPINELLI, W. R.—GARCIA, A.: Mater. Sci. Eng. A, *421*, 2006, p. 245.
[20] KIRKWOOD, D. H.: Mater. Sci. Eng. A, *73*, 1985, p. 1. doi:10.1016/0025-5416(85)90319-2